

Constraining the initial conditions of globular clusters using their radius distribution

Poul E. R. Alexander^{1*} and Mark Gieles^{1,2}

¹*Institute of Astronomy, University of Cambridge, Madingley Road, Cambridge, CB3 0HA, UK*

²*Department of Physics, University of Surrey, Guildford, GU2 7XH, UK*

Accepted 2013 February 09; Received 2013 February 08; in original form: 2013 January 21

ABSTRACT

Studies of extra-galactic globular clusters have shown that the peak size of the globular cluster (GC) radius distribution (RD) depends only weakly on galactic environment, and can be used as a standard ruler. We model RDs of GC populations using a simple prescription for a Hubble time of relaxation driven evolution of cluster mass and radius, and explore the conditions under which the RD can be used as a standard ruler. We consider a power-law cluster initial mass function (CIMF) with and without an exponential truncation, and focus in particular on a flat and a steep CIMF (power-law indices of 0 and -2 , respectively). For the initial half-mass radii at birth we adopt either Roche-lobe filling conditions (‘filling’, meaning that the ratio of half-mass to Jacobi radius is approximately $r_h/r_J \simeq 0.15$) or strongly Roche-lobe under-filling conditions (‘under-filling’, implying that initially $r_h/r_J \ll 0.15$). Assuming a constant orbital velocity about the galaxy centre we find for a steep CIMF that the typical half-light radius scales with galactocentric radius R_G as $R_G^{1/3}$. This weak scaling is consistent with observations, but this scenario has the (well known) problem that too many low-mass clusters survive. A flat CIMF with ‘filling’ initial conditions results in the correct mass function at old ages, but with too many large (massive) clusters at large R_G . An ‘under-filling’ GC population with a flat CIMF also results in the correct mass function, and can also successfully reproduce the shape of the RD, with a peak size that is (almost) independent of R_G . In this case, the peak size depends (almost) only on the peak mass of the GC mass function. The (near) universality of the GC RD is therefore because of the (near) universality of the CIMF. There are some extended GCs in the outer halo of the Milky Way that cannot be explained by this model.

Key words: galaxies: star clusters – globular clusters: general

1 INTRODUCTION

It has long been known that the shape of globular cluster (GC) luminosity function is relatively insensitive to galactic environment. Accordingly, the peak luminosity of $M_V \simeq -7$ is often used as a standard candle (Shapley & Sawyer 1927; Rejkuba 2012). It is however not known whether this typical luminosity is the result of dynamical evolution (Fall & Zhang 2001) or the outcome of the cluster formation process (see Brodie & Strader 2006; Portegies Zwart, McMillan, & Gieles 2010, for reviews).

Jordán et al. (2005) showed that the half-light radii (r_{hl}) of GCs are also sufficiently independent of galactic environment to be used as a standard ruler. Typical radii of $r_{hl} \simeq 3$ pc are found for clusters in the Milky Way (Harris 1996, 2010 version) and other galaxies (Kundu & Whitmore 2001; Jordán et al. 2005; Peng et al. 2011). Within galaxies the typical radii depend only weakly on galactocentric radius R_G . For the Milky Way GCs van den Bergh

et al. (1991) and McLaughlin (2000) find $R_G^{0.5}$ and $R_G^{0.4}$, respectively. Similar and shallower correlations are found for clusters in external galaxies: $r_h \propto R_G^{0.38}$ (in the Sombbrero galaxy; Spitler et al. 2006), $r_h \propto R_G^{0.17}$ (for the inner regions of NGC 5128; Gómez & Woodley 2007), $r_h \propto R_G^{0.11}$ (in a sample of six ellipticals; Harris 2009). If clusters fill their Jacobi radius r_J , their radii scale with their mass M and their orbital frequency Ω as $M^{1/3}\Omega^{-2/3}$. Hence, for a constant M and orbital velocity V_G we expect $r_{hl} \propto R_G^{2/3}$, i.e. a stronger dependence on R_G than observed.

The objective of this work is to understand how the shape of the cluster radius distribution (RD) depends on the cluster initial mass function (CIMF), the distribution of clusters within the galaxy and the initial cluster sizes. This will allow us to use the RD to put additional constraints on the initial conditions of GCs.

The structure of this paper is as follows: In Section 2 we discuss the RD arising for a synthetic sample of GCs at one R_G . In Section 3 we consider an entire population of synthetic clusters and compare our results with the Milky Way GC system. We finally

* e-mail: pera@ast.cam.ac.uk

compare our results to previous studies and provide a summary in Section 4.

2 THE RADIUS DISTRIBUTION OF CLUSTERS IN A SINGLE TIDAL ENVIRONMENT

We start by considering the radius distribution (RD), i.e. the number clusters with a half-mass radius between r_h and $r_h + dr_h$, of clusters evolving in a fixed tidal environment (for example, evolving at a constant R_G within a galaxy halo). For this situation the RD can be related to the cluster initial mass function (CIMF, i.e. the number of clusters with initial mass in the interval M_0 and $M_0 + dM_0$) as

$$\frac{dN}{dr_h}(R_G) = \frac{dN}{dM_0} \left| \frac{\partial M_0}{\partial M} \right| \left| \frac{\partial M}{\partial r_h}(R_G) \right|. \quad (1)$$

Here $|\partial M_0/\partial M|$ and $|\partial M/\partial r_h(R_G)|$ depend on the mass and radius evolution, respectively. These will be discussed in the following sections.

2.1 Initial mass function and mass evolution

In this section we assume that the CIMF is a power-law distribution: $dN/dM_0 \propto M_0^\alpha$ in the range $M_{\text{low}} \leq M_0 \leq M_{\text{up}}$. In Section 3 we additionally consider Schechter (1976) distributions. We aim to reproduce the GC population of a Milky Way like galaxy, and therefore adopt a constant $V_G = 220 \text{ km s}^{-1}$ such that $\Omega \propto R_G^{-1}$. Throughout this work we assume that clusters evolve with a constant mass-loss rate that depends on the galactocentric radius as $\dot{M}R_G = -20 M_\odot \text{ Myr}^{-1} \text{ kpc}$ (Gieles, Heggie, & Zhao 2011). The mass then evolves as

$$M = M_0 - \Delta, \text{ with } \Delta \equiv -\dot{M}t \propto R_G^{-1}. \quad (2)$$

Here, t is the age of the cluster, for which we adopt 13 Gyr throughout this work. We then have $|\partial M_0/\partial M| = 1$. The total lifetime, or dissolution time, is $t_{\text{dis}} = -M_0/\dot{M}$. For the final term of equation (1), we need to know how the radii of clusters depend on M , for which we compare two different scenarios. In Section 2.2, we consider Roche-lobe filling clusters, whereby the ratio of half-mass to Jacobi radius ($\mathcal{R} \equiv r_h/r_J$) is constant and approximately the Hénon (1961) value, $\mathcal{R} = 0.145$. In Section 2.3, we consider initially Roche-lobe under-filling clusters, where initially $\mathcal{R} = 0$ and \mathcal{R} increases during the evolution.

2.2 Roche-lobe filling clusters

We first consider the scenario whereby all clusters fill their Roche-lobe from birth. Such clusters will evolve at a constant density whilst losing mass (Hénon 1961) and so

$$M = Ar_h^3, \text{ with } A \equiv \frac{2\Omega^2}{GR^3} \propto R_G^{-2}, \quad (3)$$

where G is the gravitational constant. From this we find $|\partial M/\partial r_h(R_G)| \propto r_h^2 R_G^{-2}$, which we combine with equation (1) to derive the RD

$$\frac{dN}{dr_h}(R_G) \propto (Ar_h^3 + \Delta)^\alpha r_h^2 R_G^{-2} \propto \begin{cases} r_h^2 R_G^{-(2+\alpha)} & , 0 \leq Ar_h^3 \lesssim \Delta, \\ r_h^{3\alpha+2} R_G^{-2(\alpha+1)} & , \Delta \lesssim Ar_h^3 \leq M_{\text{up}}. \end{cases} \quad (4)$$

For $\alpha = 0$ the RD is a single power-law with slope $+2$, while for $\alpha \neq 0$ it is a double power-law distribution: at small radii the shape of the RD is independent of the shape of the CIMF and only depends on how clusters lose mass. This is because the Globular Cluster Mass Function (GCMF) evolves to $dN/dM \simeq \text{constant}$ at low masses, regardless of the shape of the CIMF (Hénon 1961; Fall & Zhang 2001). At large radii the shape of the RD depends on the index of the CIMF, for which we find two regimes: firstly, for $\alpha < -2/3$ the RD is an decreasing function of r_h and the peak of the distribution occurs where the two power-laws join, i.e. at $\hat{r}_h \simeq (\Delta/A)^{1/3} \propto R_G^{1/3}$, where we introduce the symbol \hat{r}_h to denote the mode of the RD (most probable radius). For $\alpha > -2/3$ the RD rises until the largest radius present, which is the radius of the most massive cluster (M_{up}) and thus $\hat{r}_h \propto R_G^{2/3}$.

2.3 Roche-lobe under-filling clusters

We next consider clusters that are born Roche-lobe under-filling. We use the model of Gieles et al. (2011) for the relaxation driven evolution of r_h as a function of M_0 and R_G , in which clusters are assumed to form with a half-mass density much greater than the tidal density. In the first (roughly) half of their life clusters expand and become increasingly Roche-lobe filling, while in the second half they contract at a constant density, and near final dissolution the radius evolves as in equation (3) from Section 2.2.

The functional form for the evolution of r_h is (equation (26) in Gieles et al. 2011)

$$r_h = \left(\frac{M}{A}\right)^{1/3} \left(1 - \left[\frac{M}{M_0}\right]^{5/2}\right)^{2/3}. \quad (5)$$

Note that $A = A(R_G)$, $M = M(M_0, \Delta)$ and $\Delta = \Delta(R_G, t)$. In the late stages of evolution ($M \ll M_0$), this function converges to the Roche-lobe filling relation (equation 3). Meanwhile, for $M \simeq M_0$ we find $r_h \propto M_0^{-1/3} t^{2/3}$, which follows from the fact that in the expansion phase clusters evolve toward a constant ratio of τ_{rh}/t with $\tau_{\text{rh}} \propto (Mr_h^3)^{1/2}$ (assuming a constant mean stellar mass and Coulomb logarithm, Spitzer & Hart 1971). If there are clusters in both the expansion and contraction phases, the size of the largest cluster (r_h^{max}) is not that of the most massive cluster, as was the case for Roche-lobe filling clusters (Section 2.2). To find r_h^{max} in a population of clusters with different M_0 at a given R_G and t , we numerically solve $dr_h/dM_0 = 0$ (equation 5), and find $M_0(r_h = r_h^{\text{max}}) \simeq 3.175\Delta$. We note that this is *not* the mass of the cluster that has just reached its maximum size, but instead a slightly more massive cluster that is still expanding (see Fig. 1). This is because the maximum r_h is reached roughly half-way the total lifetime (Gieles et al. 2011), so the cluster that has reached its maximum size has an initial mass of $M_0 \simeq 2\Delta$. From Fig. 1 we also see that clusters can be placed in three categories, which we base on the their M_0 :

- (i) $M_0 \leq 2\Delta$ – clusters have past their individual maximum r_h and are now approximately Roche-lobe filling (dashed/green tracks).
- (ii) $2\Delta < M_0 \leq 3.175\Delta$ – clusters that are expanding toward their individual maximum r_h , and show a positive correlation between mass and r_h (solid/magenta tracks).
- (iii) $M_0 > 3.175\Delta$ – clusters that are expanding, and have a negative correlation between M and r_h (dot-dashed/cyan tracks).

We cannot derive an easy analytical expression for the RD, because we can not invert the relation $r_h(M_0)$ (equation 5). We are

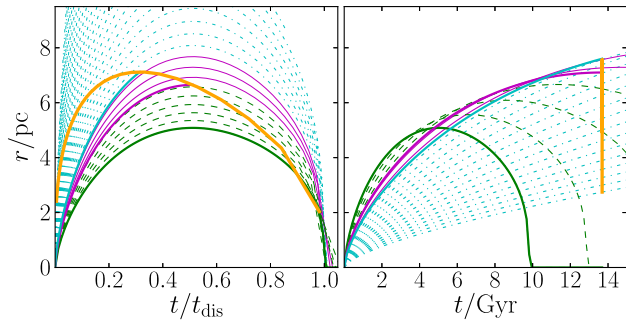


Figure 1. Radius evolution of clusters of different masses ($10^4 M_\odot < M < 10^7 M_\odot$) at $R_G = 8.5$ kpc, $V_G = 220$ km s $^{-1}$, as a function of fractional dissolution time (left panel) and physical time (right panel). The thick/orange line represents the r_h of clusters after a Hubble time, and is curved in the left panel on account of the longer t_{dis} of more massive clusters. The green/dashed, magenta/solid and cyan/dot-dash lines represent the evolutionary tracks of individual (sample) clusters in states (i), (ii) and (iii), respectively. These tracks are thicker for evolution that has occurred during a Hubble time, that is, on the left of the orange line.

however able to give the behaviour of the RD at the extremes of r_h . For expanding clusters, we use $r_h \propto M_0^{-1/3}$ and $M \simeq M_0$ to find $|\partial M/\partial r_h| \propto r_h^{-4}$, while contracting clusters approximately follow the same relationships as in Section 2.2. We substitute these expressions into equation (1) and find

$$\frac{dN}{dr_h}(R_G) \propto \begin{cases} r_h^2 R_G^{-(2+\alpha)} & , 0 \lesssim r_h \lesssim r_h^{\text{max}}, \\ r_h^{-(3\alpha+4)} & , r_h(M_{\text{up}}) \leq r_h \lesssim r_h^{\text{max}}. \end{cases} \quad (6)$$

Here we assumed that clusters with $M = M_{\text{low}}$ have dissolved already and that r_h shrinks to 0 near dissolution. These two parts of the RD both occupy the region $0 \lesssim r_h \lesssim r_h^{\text{max}} \propto R_G^{1/3}$. The first approximation applies to the clusters whose r_h has approximately reached the Roche-lobe filling condition ($\mathcal{R} \simeq 0.145$), i.e. $M_0 \lesssim 3.175\Delta$, while the second approximation holds for the expanding clusters ($M_0 \gtrsim 3.175\Delta$). For $\alpha = -2$ we find that both extremes of the RD behave as r_h^2 . For very high M_{up} (where $r_h(M_{\text{up}}) \simeq 0$), this RD has the same shape as the RD for Roche-lobe filling clusters with $\alpha = 0$ (Section 2.2), but has a smaller r_h^{max} .

As for the Roche-lobe filling case, the mode of the RD is either at the radius of the most massive cluster or at the radius of the cluster with $M_0 \simeq \text{few} \times \Delta$, depending on whether the RD of expanding clusters is rising or falling. The difference with the Roche-lobe filling case is that $r_h(M_{\text{up}})$ is smaller than r_h^{max} . For $\alpha > -4/3$ the RD of the Roche-lobe filling clusters is rising and $\hat{r}_h = r_h^{\text{max}} \propto R_G^{1/3}$. For $\alpha < -4/3$ this part of the RD is a declining function, and if the most massive cluster is still expanding the RD peaks at the radius of the most massive cluster: $\hat{r}_h = r_h(M_{\text{up}}) < r_h^{\text{max}} = \text{constant}$ (Fig. 2). This is the most straightforward way to explain a near universal radius scale for GCs. The condition that the most massive clusters have not yet expanded until their $r_h \simeq \mathcal{R}r_J$ is not satisfied in strong tidal fields, and will be discussed further in Section 3.4.

The RD is computed for Roche-lobe under-filling clusters and for three values of α using a Monte Carlo approach (Fig. 2). The power-law behaviours at the expanding and contracting extremes are shown as dashed/black and dotted/red lines, respectively. The power-laws do not follow the Monte Carlo data where $r_h \simeq r_h^{\text{max}}$, as here $M_0 \simeq 3.175\Delta$ and mass loss is neither dominant nor negligible.

Now we have explored the different scenario for clusters at a

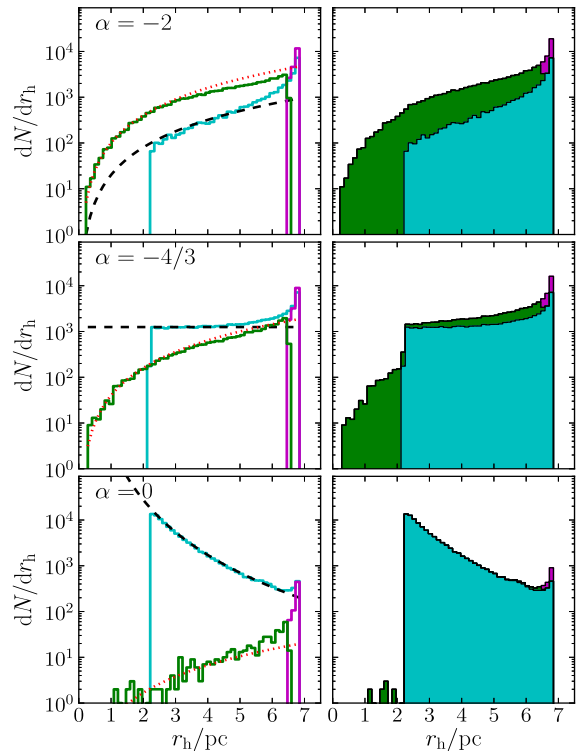


Figure 2. Monte Carlo simulations of clusters with different CIMF slopes (α) at $R_G = 8.5$ kpc with $V_G = 220$ km s $^{-1}$. The colour coding is the same as in Fig. 1 (green = stage (i) clusters, magenta = stage (ii) clusters, cyan = stage (iii) clusters). In the left panels, clusters in the three phases of evolution are shown separately, while they are added in the right panels. The dashed/black line represents the expected slope of expanding clusters while the dotted/red line corresponds to the expected slopes of approximately Roche-lobe filling (contracting) clusters (equation 6). The sample size is 10^5 clusters and clusters are evolved for 13 Gyr.

single R_G we will consider GC populations in a Milky Way type galaxy in the next section.

3 RADIUS DISTRIBUTION OF A CLUSTER SYSTEM

In this section we consider the RD of clusters in a Galactic halo, i.e. with a range of R_G . The RD can be found by multiplying the RD at a single R_G with the number of clusters at each R_G ($dN/dR_G = 4\pi R_G^2 n(R_G)$, where $n(R_G)$ is the number density of clusters in the halo) and integrating over all R_G

$$\frac{dN}{dr_h} = \int_{R_G^{\text{min}}}^{R_G^{\text{max}}} \frac{dN}{dr_h}(R_G) \frac{dN}{dR_G} dR_G. \quad (7)$$

The analytic evaluation of this integration gives results only for a limited number of cases, so we proceed by generating RDs in a Monte Carlo fashion. We therefore perform a number of simulations, for which we adopt a Hernquist (1990) model (i.e., a double power-law density profile with an r^{-1} central cusp and an r^{-4} outer halo) with a scale radius $a = 5$ kpc and a truncation at $R_G = 100$ kpc for the distribution of clusters in the Galaxy ($n(R_G)$), which is a reasonable approximation for GCs in the Milky Way (McLaughlin 2000). For the CIMF we use a Schechter (1976) function: $dN/dM_0 \propto M_0^\alpha \exp(-M_0/M_*)$, with $M_* = 10^6 M_\odot$ and $M_{\text{low}} = 100 M_\odot$. For the slope we consider $\alpha = -2$, i.e. what

is found for young clusters (Zhang & Fall 1999; Portegies Zwart et al. 2010) and $\alpha = 0$, which describes the MF of old clusters in the Milky Way and early type galaxies in the Virgo Cluster (Jordán et al. 2007). A CIMF with $\alpha = 0$ is invariant under mass-loss (Jordán et al. 2007) so at an age of 13 Gyr the GCMF has the same shape as the CIMF. The resulting RDs and the $\hat{r}_h(R_G)$ relations for these four cases are shown in Fig. 3 and are discussed below. We compare all these simulations to the r_h values of Milky Way GCs compiled from the (Harris 1996, 2010 version) catalogue. Values for r_h are derived by multiplying the observed half-light radii by 4/3 to correct for the effect of projection.

3.1 Scenario A: Roche-lobe filling clusters and $\alpha = -2$

We first consider Roche-lobe filling clusters and a CIMF with slope $\alpha = -2$. We recall from Section 2.2 that for Roche-lobe filling clusters there is a critical value for the CIMF slope of $\alpha = -2/3$: a steeper CIMF gives rise to a double power-law RD, rising at small radii and falling at large radii. The total RD is the sum of many such functions, and therefore has a (logarithmic) slope of +2 at small radii. At large radii the integration of equation (7) gives a slope of $3\alpha + 3.5 = -2.5$. The typical radius scales as $\hat{r}_h \propto R_G^{1/3}$. We recall from Section 2.2 that this is due to the scaling of the break in the double power-law RD with R_G . This scaling is close to what is found for Milky Way GCs, but in this scenario there are too many large clusters (see panel A, Fig. 3). In addition, too many low-mass clusters survive at large R_G in this scenario (Vesperini 2001; Gieles & Baumgardt 2008).

3.2 Scenario B: Roche-lobe filling clusters and $\alpha = 0$

For Roche-lobe filling clusters and $\alpha = 0$ the RD at a single R_G is simply a +2 power-law. In this case the integration of equation (7) can be performed, with the result that at large radii we find $dN/dr_h \propto r_h^{-1}$. Because of this slow decline, this scenario produces even more large clusters than scenario A. However, owing to the invariance of this CIMF under the influence of mass-loss, this scenario does predict the correct GCMF (meaning that the peak mass, \hat{M} , is independent of R_G , Vesperini 2000). Because \hat{r}_h scales with the Jacobi radius of the most massive cluster (Section 2.2) at any given R_G , we find $\hat{r}_h \propto R_G^{2/3}$ (see panel B, Fig. 3), which is a stronger correlation than found for Galactic clusters. We note that this is the only scenario out of the four we considered for which the $R_G^{2/3}$ scaling is found.

3.3 Scenario C: Roche-lobe under-filling and $\alpha = -2$

For under-filling clusters with a steep CIMF ($\alpha = -2$) both the expanding and contracting clusters have a RD that behaves as a +2 power-law (just as in scenario B). However, the total RD is different because the typical radius scales with $\hat{r}_h \propto r_h^{\max}$ and therefore $\hat{r}_h \propto R_G^{1/3}$ (Section 2.3). Accordingly, there are fewer large clusters in this scenario, because high mass clusters are still expanding to their tidal boundary and are smaller than clusters of equivalent mass in scenario B.

3.4 Scenario D: Roche-lobe under-filling and $\alpha = 0$

In the final scenario (under-filling clusters with $\alpha > -4/3$) the sample population contains a fraction of expanding clusters, which

is larger for higher values of α (Fig. 1). The radii of expanding clusters are independent of their local tidal field and also independent of their initial radii (Hénon 1965; Gieles et al. 2010). This is the case for $R_G \gtrsim 5$ kpc (panel D, Fig. 3). The typical r_h is then simply the radius of the cluster with the typical mass. For $R_G < 5$ kpc, the majority of clusters have expanded to become Roche-lobe filling and are therefore described by scenario B with a typical radius scaling as $\hat{r}_h \propto R_G^{1/3}$. The number of clusters in this regime depends on the slope of the CIMF and the Hernquist scale radius. This scenario is the only scenario that produces a clear peak in the radius distribution below 5 pc, and the only scenario to produce a rapid decline in the RD at high r_h consistent with Milky Way GCs.

3.5 Comparison to Milky Way GCs

In the right panels of Fig. 3 we show the RD and the individual r_h against R_G values of the MW GCs. The width of the Milky Way GC RD is narrow, with radii rarely in excess of 20 pc (90% of the GCs have radii < 10 pc, Harris 1996, 2010 version). Comparing this to the models we see that in Scenarios A, B there are too many clusters with $r_h \gtrsim 20$ pc (see Fig. 3), especially in scenario B, where we find clusters with size up to $r_h \sim 100$ pc. Scenarios C and D both show a narrower range of r_h , in better agreement with that found for Milky Way GCs, with scenario D providing a very comparable shape overall.

Several MW GCs at high R_G are larger than those predicted. These outlying clusters cannot be explained by our simple model for cluster evolution, and so may result from effects neglected by this study (e.g., these clusters may be accreted, or perturbed by the tidal fields of external galaxies). The scaling of \hat{r}_h with R_G of the Milky Way GCs shows considerable scatter, but is approximately $r_h \propto R_G^{0.4}$, similar to the scalings of scenarios A and C and shallower than scenario B. However, the majority of Milky Way clusters are found within the innermost ~ 10 kpc. In this regime the radii in scenario D are similar to those in C. It is therefore difficult to satisfactorily distinguish which scenario optimally represents the r_h scaling of Milky Way clusters, but combined with the superior match of the RD shape we conclude that scenario D is preferred. The $r_h(R_G)$ relationship of scenario D is also similar to that described for M87 in Webb et al. (2012). We therefore conclude that the good match of the shape of the RD in scenario D suggests that most clusters form Roche-lobe under-filling, and with a relatively flat CIMF, similar to the present day GCMF.

4 SUMMARY AND DISCUSSION

We have investigated the radius distribution (RD) of globular cluster (GC) populations in Milky Way-type haloes for a variety of initial conditions for the masses and radii. We find that Roche-lobe filling initial conditions results in too many large clusters ($\gtrsim 20$ pc) at large R_G , for both steep and shallow cluster initial mass function (CIMFs). Models in which clusters are initially Roche-lobe under-filling and form with a steep CIMF show a scaling of $\hat{r}_h \propto R_G^{1/3}$, roughly consistent with Milky Way GCs, but the shape of the synthetic RD is wider than the observed one. The mode of the half-mass RD of a GC population is independent of Galactic environment only if clusters form Roche-lobe under-filling, and with a relatively flat CIMF.

Alternative models to explain the characteristic GC radius of a few pc exist (e.g. Jordán et al. 2005; Harris et al. 2010). In these

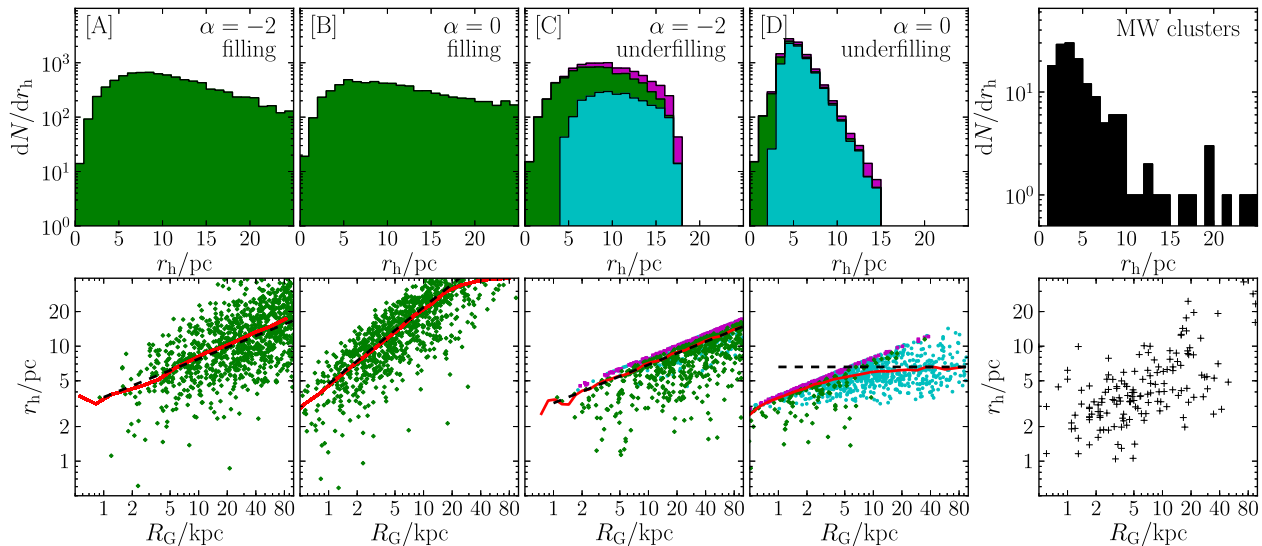


Figure 3. Monte Carlo samples of $N = 10^4$ (surviving) star clusters at $t = 13$ Gyr within an isothermal galactic halo. Clusters are simulated with a Hernquist (1990) distribution of galactocentric radii and a Schechter (1976) CIMF (see text for parameters). In the top row cyan, magenta and green regions correspond to clusters undergoing the three evolutionary stages outlined in Section 2, whilst in the bottom row individual sample clusters are denoted by green diamonds (stage (i) clusters), magenta squares (stage (ii) clusters), or cyan dots (stage (iii) clusters). The left hand panels represent scenarios A, B, C, and D as labeled, while the rightmost figure corresponds to the present day Milky Way GC population compiled from Harris (1996, 2010 version). The red solid line in the bottom row is the median r_h as a function of R_G , while the black (dotted) lines represent $r_h = \text{const}$, $r_h \propto R_G^{1/3}$, and $r_h \propto R_G^{2/3}$ as appropriate.

models the present day size is the result of the star formation process or the gas expulsion scenario, respectively. The subsequent Hubble time of evolution is assumed not to significantly change the radii of GCs. In our model scenario D, however, the typical GC size is the natural outcome of a Hubble time of dynamical relaxation and is not sensitive to the exact initial conditions or early evolution since the relaxation driven expansion erases the initial properties of the clusters (in terms of r_h , Hénon 1965).

In addition to these works, Madrid et al. (2012) show (via N -body studies) that the radius is set “by clusters that are originally massive enough to survive mass loss due to tidal stripping”. Thus, the present day radii in their model depends only on clusters’ ability to survive in the Galactic tidal field. They consider clusters at different R_G , all with the same mass and r_h . Their final r_h vs. R_G relation (their Fig. 3) is very similar to our $r_h(R_G)$ relation found in our scenario D. The radii of their clusters at large R_G are larger, because they consider clusters with lower masses which have expanded more (Hénon 1965).

In contrast to our results, Shin et al. (2013) find from a large suite of Fokker-Planck simulations that models in which GCs are on average larger than at the present fit the data best. A fraction of their clusters are Roche-lobe overflowing at birth. Because their result is based on χ^2 fits against the entire GC population, excluding accreted clusters, their fit results are mainly driven by clusters in the inner parts of the Milky Way. Also in our scenario D most clusters at $R_G \lesssim 5$ kpc have filled their Roche-lobes and it is hard to distinguish scenarios there. Analyses of the orbits and radii of GCs suggests that a large fraction of them are Roche-lobe filling at the present day (e.g., Baumgardt et al. 2010; Ernst & Just 2013), supporting our conclusion that most clusters started more compact. Shin et al. (2013) find that the CIMF must have been flat, in agreement with what we find. The flat CIMF needed to get the shape of the RD right is in stark contrast with the observed power-law mass function of young clusters (Portegies Zwart et al. 2010) and is yet another argument that dynamical evolution cannot be responsible

for the difference (see also Vesperini 2001; Gieles & Baumgardt 2008).

For the models described in this study we assumed the *in situ* formation of the GC population. However, some of the outer halo clusters, many of which are the large outliers in the RD were most likely from dwarf satellites. A connection between dwarf galaxies and extended clusters has previously been suggested (Elmegreen 2008; Da Costa et al. 2009; Mackey et al. 2010). We have furthermore made the assumption of a constant mass-loss rate, and we omitted several physical effects such as the delayed escape of stars from the Roche-lobe (Fukushige & Heggie 2000) and stellar evolution. A fast cluster evolution code is being developed (Alexander & Gieles 2012) with the goal to include all these effects to be able to model the RD, GCMF and the R_G distribution in the future.

ACKNOWLEDGEMENTS

We thank Holger Baumgardt and Henny Lamers for insightful discussions and helpful comments. We also thank our anonymous reviewer for helpful suggestions. The authors are grateful to the Royal Society for international exchange scheme funding, and to the University of Queensland, Brisbane, where part of this study was performed. PA acknowledges financial support from STFC, and MG thanks the Royal Society for financial support.

References

- Alexander P. E. R., Gieles M., 2012, MNRAS, 2811
- Baumgardt H., Parmentier G., Gieles M., Vesperini E., 2010, MNRAS, 401, 1832
- Brodie J. P., Strader J., 2006, ARA&A, 44, 193
- Da Costa G. S., Grebel E. K., Jerjen H., Rejkuba M., Sharina M. E., 2009, AJ, 137, 4361

- Elmegreen B. G., 2008, *Ap.J.*, 672, 1006
Ernst A., Just A., 2013, *MNRAS*, 554
Fall S. M., Zhang Q., 2001, *Ap.J.*, 561, 751
Fukushige T., Heggie D. C., 2000, *MNRAS*, 318, 753
Gieles M., Baumgardt H., 2008, *MNRAS*, 389, L28
Gieles M., Baumgardt H., Heggie D. C., Lamers H. J. G. L. M., 2010, *MNRAS*, 408, L16
Gieles M., Heggie D. C., Zhao H., 2011, *MNRAS*, 413, 2509
Gómez M., Woodley K. A., 2007, *Ap. J. Letters*, 670, L105
Harris W. E., 1996, *AJ*, 112, 1487
Harris W. E., 2009, *Ap.J.*, 699, 254
Harris W. E., Spitler L. R., Forbes D. A., Bailin J., 2010, *MNRAS*, 401, 1965
Hénon M., 1961, *Annales d'Astrophysique*, 24, 369
Hénon M., 1965, *Annales d'Astrophysique*, 28, 62
Hernquist L., 1990, *Ap.J.*, 356, 359
Jordán A. et al., 2005, *Ap.J.*, 634, 1002
Jordán A. et al., 2007, *Ap.J. Supplements*, 171, 101
Kundu A., Whitmore B. C., 2001, *AJ*, 121, 2950
Mackey A. D. et al., 2010, *Ap. J. Letters*, 717, L11
Madrid J. P., Hurley J. R., Sippel A. C., 2012, *Ap.J.*, 756, 167
McLaughlin D. E., 2000, *Ap.J.*, 539, 618
Peng E. W. et al., 2011, *Ap.J.*, 730, 23
Portegies Zwart S. F., McMillan S. L. W., Gieles M., 2010, *ARA&A*, 48, 431
Rejkuba M., 2012, *Ap&SS*, 341, 195
Schechter P., 1976, *Ap.J.*, 203, 297
Shapley H., Sawyer H. B., 1927, *Harvard College Observatory Bulletin*, 852, 22
Shin J., Kim S. S., Yoon S.-J., Kim J., 2013, *Ap.J.*, 762, 135
Spitler L. R., Larsen S. S., Strader J., Brodie J. P., Forbes D. A., Beasley M. A., 2006, *AJ*, 132, 1593
Spitzer L. J., Hart M. H., 1971, *Ap.J.*, 164, 399
van den Bergh S., Morbey C., Pazder J., 1991, *Ap.J.*, 375, 594
Vesperini E., 2000, *MNRAS*, 318, 841
Vesperini E., 2001, *MNRAS*, 322, 247
Webb J. J., Sills A., Harris W. E., 2012, *Ap.J.*, 746, 93
Zhang Q., Fall S. M., 1999, *Ap. J. Letters*, 527, L81